Displacements and transformations of nitrate-rich and nitrate-poor water masses in the tropical Pacific during the 1997 El Niño

Marie-Hélène Radenac, Yves Dandonneau, Bruno Blanke

Displacements and transformations of nitrate-rich and nitrate-poor water masses in the tropical Pacific during the 1997 El Niño

MARIE-HELENE RADENAC(✉)

Laboratoire d'Études en Géophysique et Océanographie Spatiale CNRS-IRD-UPS-CNES, 14 avenue Édouard Belin, 31401 Toulouse cedex 9, France

e-mail: marie-helene.radenac@cnes.fr
phone: (33) 5 61 33 30 00
fax: (33) 5 61 25 32 05

YVES DANDONNEAU

IPSL, Laboratoire d'Océanographie Dynamique et de Climatologie CNRS-IRD-UPMC, case 100, 4 place Jussieu, 75252 Paris cedex 05, France

BRUNO BLANKE

Laboratoire de Physique des Océans, UFR Sciences et Technique CNRS-IFREMER-UBO, 6 avenue Le Gorgeu, BP 809, 29285 Brest, France

Submitted to Ocean Dynamics: August 27th, 2004
Revised: December 7th, 2004

Abstract A Lagrangian analysis was applied to the outputs of a coupled physical-biogeochemical model to describe the redistribution of nitrate-rich and nitrate-poor surface water masses in the tropical Pacific throughout the major 1997 El Niño. The same tool was used to analyze the causes of nitrate changes along trajectories and to investigate the consequences of the slow nitrate uptake in the High Nutrient Low Chlorophyll (HNLC) region during the growth phase of the event. Three patterns were identified during the drift of water masses. The first mechanism is well known along the equator: oligotrophic waters from the western Pacific are advected eastward and conserve their oligotrophic properties along their drift. The second one concerns the persistent upwelling in the eastern basin. Water parcels have complex trajectories within this retention zone and remain mesotrophic. This study draws attention to the third process which is very specific to the HNLC region and to the El Niño period. During the 1997 El Niño, horizontal and vertical inputs of nitrate decreased so dramatically that nitrate uptake by phytoplankton became the only mechanism driving nitrate changes along pathways. The study shows that because of the slow nitrate uptake characteristic of the tropical Pacific HNLC system, nitrate of the pre-El Niño photic layer can support biological production for a period of several months. As a consequence, the slow nitrate uptake delays the gradual onset of poor conditions over near all the area usually occupied by upwelled waters. Owing to this process, mesotrophic conditions persist in the tropical Pacific during El Niño events.

Keywords *nitrate uptake* *tropical Pacific* *El Niño* *Lagrangian analysis*

1 Introduction

Nitrate-rich waters of the equatorial divergence in the eastern tropical Pacific are surrounded by oligotrophic regions: the warm pool to the west and the subtropical gyres north and south.

In the photic layer of the equatorial divergence, the phytoplankton biomass is low relative to available nitrate concentrations. High Nutrient Low Chlorophyll (HNLC) conditions persist because the ecosystem is iron-limited and grazing-balanced (Landry et al. 1997). Biologically available iron in the photic layer is mainly upwelled from the Equatorial Undercurrent (EUC) (Coale et al. 1996). The overall consequences of such an ecosystem are that nitrate uptake is kept at a very low rate (Price et al. 1994) and that a large amount of surface nitrate remains unused in surface water (Coale et al. 1996; Landry et al. 1997).

The northern limit of the enriched waters of the equatorial divergence is sharply defined around 5°N (Wyrtki and Kilonsky 1984; Bender and McPhaden 1990). The surface waters of the tropical part of the north Pacific gyre are nitrate-depleted with low phytoplankton biomass (Wyrtki and Kilonsky 1984; Hardy et al. 1996). The deep chlorophyll maximum is close to the nitracline at about 100 m depth (Karl and Lukas 1996).

South of the HNLC waters of the equatorial divergence, the tropical gyre is probably among the most undersampled regions. Cruise surveys have shown a deep nitrate-depleted surface layer with low chlorophyll concentration (Dandonneau 1979; Wyrtki and Kilonsky

1984; Hardy et al. 1996; Raimbault et al. 1999). Chlorophyll- and nutrient-rich surface water as far south as 12°S is a frequent feature (Wyrtki and Kilonsky 1984; Dandonneau and Eldin 1987; Bender and McPhaden 1990; Raimbault et al. 1999) and the transition between the enriched and oligotrophic waters is more gradual than at the northern limit.

West of the equatorial divergence, the transition toward the warm pool is marked by a sharp salinity front while the sea surface temperature increases smoothly (Kuroda and McPhaden 1993; Eldin et al. 1997). This is also the site of transition between the HNLC and oligotrophic equatorial ecosystems producing a discontinuity of chemical and biological properties such as nutrients, chlorophyll, zooplankton biomass, pCO_2, phytoplankton community (Inoue et al. 1996; Eldin et al. 1997; Boutin et al. 1999; Le Borgne et al. 2002; Kobayashi and Takahashi 2002). Mean zonal currents approach zero in this region of water convergence (Picaut et al. 1996). Warm pool waters, defined by temperature greater than 29°C (McPhaden and Picaut 1990), are nitrate and chlorophyll-depleted with very low new production. The nitracline, the chlorophyll maximum and a weak new production maximum are closely associated with the thermocline at a depth of around 100 m (Mackey et al. 1995; Radenac and Rodier 1996; Navarette 1998).

Biogeochemical conditions in the tropical Pacific change drastically during El Niño events. These changes are generally understood to be a collapse of primary production in the entire equatorial cold tongue (Barber and Chavez, 1983; Strutton and Chavez 2000). Measurements relying on oceanographic cruises, merchant ships, moorings, as well as model studies have revealed changes in the east-west equatorial asymmetry of nutrients and biology. Nevertheless, it was during the 1997-1998 event that this impact was first visualized on the tropical Pacific basin scale owing to the timely launches of new ocean color sensors (Fig. 1). The Polarization and Directionality of the Earth Reflectances (POLDER) (Deschamps et al. 1994) sensor aboard the ADEOS satellite provided data (November 1996-June 1997) before and during the early phase of the event. The Sea-viewing Wide Field-of-view Sensor (SeaWiFS) (McClain et al. 1998) mission started in September 1997 and captured the warm phase. Fig. 1 summarizes the evolution of the 1997 El Niño event as observed by ocean color sensors. Before the onset of the event, weak La Niña conditions prevailed in the tropical basin in late 1996 (Fig. 1a) and chlorophyll rich waters (Muramaki et al. 2000; Radenac et al. 2001; Ryan et al. 2002) extended across most of the equatorial basin. In May 1997, the satellite chlorophyll (Fig. 1b) had fallen by about 50% since November 1996 and reached about 0.1 mg m^{-3} in the western part of the equatorial cold tongue. East of 160°W however, the surface chlorophyll remained close to the November 1996 values (about 0.2 mg m^{-3}). During

the peak of the event, from November 1997 to January 1998 (Fig. 1c), more than six months after the El Niño event started, the chlorophyll rich region was reduced to its narrowest zonal extent (Radenac et al. 2001) and high chlorophyll waters stretch from the Central American coast to the equatorial western basin (Murtugudde et al. 1999). Unfortunately, there was a three-month gap (July to September 1997) in the time series of sea color data that corresponded to an essential transition phase of the onset of El Niño.

What were the processes that led to the December 1997 biological situation as revealed by ocean color sensors in the tropical Pacific (Fig. 1c)? Most previous studies focused on the equatorial zone. Observations and simulations have shown that the variability of nitrate, chlorophyll or new production is mainly controlled by the fast equatorial dynamics (Chavez et al. 1998; Stoens et al. 1999; Friedrichs and Hofmann 2001; Radenac et al. 2001) and their analyses stressed the abrupt decrease of primary production. They did not closely examine the off-equatorial situation for which we hypothesize here that the low nitrate uptake rate caused by the HNLC ecosystem should delay the setting up of oligotrophic conditions that characterize El Niño. In this study, a Lagrangian analysis (Blanke and Raynaud 1997) was applied to the outputs of a physical-biogeochemical model (Radenac et al. 2001) to address the following two issues. First, the goal was to describe the redistribution of surface water masses in the tropical basin during the 1997 El Niño and secondly, to investigate the role of the slow nitrate uptake in the HNLC region during the growth phase of the event.

2 Numerical tools and data

2.1 The physical-biological model

The primitive equation general circulation model (GCM) (Maes et al. 1997; Vialard et al. 2001) covers the tropical Pacific between 120°E and 75°W and between 30°N and 30°S. The zonal resolution is 1° and the meridional resolution, close to 0.5° between 5°N and 5°S, increases to 2° at the northern and southern boundaries. The vertical resolution is 10 m over the first 150 m in depth. Wind stress data derived from the ERS1-2 scatterometer are used to force the model during the 1993-1998 period. Estimates of the heat and freshwater fluxes are computed from the 1979-1993 seasonal cycle of the ECMWF reanalysis. The modeled heat flux is parameterized following Vialard et al. (2001). The long term SST drift is counterbalanced by a -40 W m^{-2} K^{-1} relaxation (with a relaxation timescale of 50 days for a 40 m layer) toward the observed Reynolds and Smith (1994) sea surface temperature. A

correction term derived as by Vialard et al. (2002) is also applied to the freshwater flux to avoid the sea surface salinity drift inherent in the forcing freshwater flux.

Five-day outputs of the ocean circulation model (zonal velocity u, meridional velocity v, vertical velocity w, vertical diffusion coefficient K_z) and the same horizontal eddy coefficient K_h as in the GCM force the nitrate advection-diffusion equation:

$$\partial_t NO_3 = -u\partial_x NO_3 - v\partial_y NO_3 - w\partial_z NO_3 + K_h \Delta_h (NO_3) + \partial_z (K_z \partial_z NO_3) + S \quad (1)$$

in which the left-hand side represents the local nitrate change. The first three terms on the right-hand side are the zonal, meridional and vertical advection, respectively. The fourth and fifth terms are the horizontal diffusion (parameterized by the horizontal Laplacian operator Δ_h) and the vertical diffusion.

In the euphotic layer, the biological model consists of a nitrate uptake S (new production) that is biomass-dependant (Price et al. 1994; Landry et al. 1997):

$$S = -V_{max} \frac{NO_3}{NO_3 + K_{NO_3}} \frac{PUR}{PUR + K_E} [Chl] \quad (2)$$

in which both the nitrate and light limitations terms are expressed in Michaelis-Menten form. The photosynthetic usable radiation (*PUR*) is deduced from the short wave downward radiation as explained by Stoens et al. (1999) and K_E (70×10^{-6} mol photon m^{-2} s^{-1}) is the half saturation constant for *PUR*. The maximum nitrate uptake rate V_{max} (3×10^{-3} μmol N mg Chl^{-1} s^{-1}) and the half saturation concentration K_{NO3} (0.01 μM) have been adjusted in such a way that modeled nitrate fields agree the best with concurrently observed vertical sections of nitrate content. Because this model does not explicitly resolve variations in biomass, a calculation specific to the tropical Pacific is applied to chlorophyll profiles empirically derived from modeled nitrate at the surface (Stoens et al. 1999). New production is locally exported (exponential shape as by Honjo, 1978, with a 120m length scale) below the photic layer and is instantaneously remineralized into nitrate. Details on the choice of constants and rationale of the biological model are given in Stoens et al. (1999) and Radenac et al. (2001).

2.2 The Lagrangian tool

The Lagrangian approach described in detail by Blanke and Raynaud (1997) is applied to the physical-biological model outputs. Streamlines are computed from the archived, three-dimensional velocity field (5-day running means). Assuming that the velocity is stationary

over each successive sampling period, consecutive portions of streamlines represent the trajectories of particles. Properties along trajectories are interpolated from modeled three-dimensional fields. Both direct and reverse (finding the origin of water mass) experiments can easily be performed because it is an off-line technique.

In a Lagrangian form, the equation of conservation of nitrate is:

$$d_t NO_3 = K_h \Delta_h (NO_3) + \partial_z (K_z \partial_z NO_3) + S \qquad (3)$$

in which the nitrate change along the trajectory ($d_t NO_3$) corresponds to the effect of the horizontal and vertical diffusions and of the nitrate sink S (eq. 2). For off-line diagnostics, this relation is still valid if we assume that unsampled tracer and velocity fluctuations are small relative to their mean values on the time scale of the model outputs. Previous studies using a similar model (Maes et al. 1997; Lehodey et al. 1998; Stoens et al. 1999; Vialard et al. 2001; Radenac et al. 2001) have shown that five-day outputs are relevant for capturing the large-scale variability in the tropical Pacific.

The December 1997 (Fig. 1c) situation was chosen to represent the peak of the 1997 El Niño and the May 1997 situation (Fig. 1b) as the reference for the early stage of the event. At that time, the surface circulation characteristic of El Niño had clearly settled while the disruption of the east-west equatorial trophic contrast was just starting. Our Lagrangian analyses refer to these situations. The aim is to investigate the redistribution of tropical surface water masses and to explain nitrate variations along specific trajectories.

2.3 Identification of water masses

The domain was partitioned into seven water masses essentially based on the nitrate distribution in May 1997 (Table 1). A 1 μM nitrate threshold discriminates oligotrophic waters from nitrate-rich waters. Among the oligotrophic surface waters, an additional temperature criterion ($T \geq 29°C$) was used to identify warm pool water and geographical limits bounded the northwest subtropical water, the northeast subtropical water and the south subtropical water. The concentration of surface nitrate-rich waters ranged between 1 and 12 μM. Geographical criteria separated the equatorial upwelled water and the coastal waters of Central and South America. Subsurface waters with nitrate concentration higher than 1 μM and that did not match the preceding criteria were also considered. These water masses will be denominated below according to their status in May 1997, even if their nitrate content (oligotrophic/mesotrophic) changes during the course of the El Niño.

2.4 Validation data

Three existing data sets were used to validate the modeled surface circulation in 1997. The first one consisted of currents data gathered twice a year during cruises undertaken to maintain the Tropical Atmosphere Ocean/Triangle Trans Ocean Buoy Network (TAO/TRITON) moorings between 165°E and 95°W (Hayes et al. 1991; McPhaden et al. 1998). During these cruises, ADCPs were operated continuously along meridional sections. The processing and gridding of these data have been described in detail by Johnson et al. (2000). In the second data set (Ocean Surface Current Analysis – Real time, OSCAR), near-surface currents were derived from satellite altimeter, scatterometer and sea surface temperature (Lagerloef et al. 1999; Bonjean and Lagerloef 2002). In this product, the 30 m surface layer current is the sum of geostrophic and Ekman currents and of a buoyancy term. It has been available since October 1992 on a 1°×1° grid with a 10-day temporal resolution. The last set of data used for of the 6-hour interpolated trajectories was collected from the satellite-tracked drifting buoys by the Atlantic Oceanographic and Meteorological Laboratory (AOML) (Pazan and Niiler 2004). These data are available on-line (http://www.aoml.noaa.gov/phod/dac/dacdata.html) and their processing has been described by Hansen and Poulain (1996).

3 Results

3.1 Surface circulation

The 'climatology' (not shown) that we derived from the modeled 15 m currents averaged over the 1993-1996 period (the 1997-1998 ENSO years were excluded because of the strong anomalies they induced) is very similar to the one presented by Vialard et al (2001; their fig. 5). Consequently, the reader is referred to Vialard et al. (2001) and Radenac et al. (2001) for a validation of the mean modeled surface currents. The salient contrast between modeled surface circulation before and during the 1997 El Niño is illustrated in fig.1. The time evolution of the zonal current along 155°W as derived from satellites and from the model is shown in fig.2. Boreal spring and fall snapshots of measured zonal velocity are also shown.

As was expected, the modeled South Equatorial Current (SEC) during cold conditions in late 1996 was stronger than average and spread well past the date line. The North Equatorial Countercurrent (NECC) was strong and extended across the basin. These features are consistent with surface currents measured during cruises or deduced from satellite data

(Lagerloef et al. 1999; Johnson et al. 2000). Between the boreal fall of 1996 and the spring of 1997, the NECC shifted southward and grew in strength (Fig. 2). Its zonal velocity peaked in the fall of 1997. At the equator, the current was mostly eastward from March to the end of the year, except in July and August. These eastward currents merged into a large eastward flow between 6°N and 2°S (Johnson et al. 2000). The model often failed to reproduce the bimodal structure of the eastward flow during the mature phase (see the November 1997 meridional profile). Actually, the eastward current at the equator was accurately simulated but the NECC was too weak. In November, the maximum zonal current measured during the cruise or derived from satellite data was close to 1 m s^{-1}, which is about twice the modeled velocity. Besides, a comparison with the TAO zonal current (not shown) shows that the model tended to overestimate the duration and westward extent of the brief-living SEC in July-August, while the satellite derived currents seem to have missed part of this event.

Trajectories of satellite-tracked drifters integrate the different circulation events that occurred during the 1997 El Niño. They resolve circulation features at a high spatial resolution of which the GCM derived trajectories are not capable. Nevertheless, their comparison reveals interesting and consistent large-scale patterns. Drifters present between 15°S and 15°N in May 1997 were selected and their displacements followed until December 1997 (Fig. 3a). The coverage is rather sparse except in the near equatorial region and in the southern hemisphere west of 140°W. To compare these observed trajectories with the modeled circulation, virtual drifters were released in the modeled velocity field at the location of the *in situ* drifting buoys (Fig. 3b): in the North Equatorial Current (NEC) region, in the near equatorial zone and in the south and south west regions. All simulated trajectories begin in early May 1997 and are integrated until December 1997 at a constant depth (15 m) in order to better represent the 15m deep circulation followed by *in situ* drifters (Niiler 2001).

The observed trajectories that start between 10°N and 15°N had roughly eastward drifts and remained within this latitude band. In the model, the zonal component of the NEC was too weak and, as a result the virtual drifters had too strong a poleward drift. A comparison with the Reverdin et al. (1994) climatology confirms the poleward trend of modeled currents in this region. Nine *in situ* drifters released in the near equatorial zone (3°S-1°N) were caught in the strong eastward surface flow that dominates over most of the equatorial basin in May and June. They separated into two groups when the SEC resumed in July. In the northern group, two of these drifters rapidly travelled eastward following the strong NECC. This pathway was well represented by the model. Virtual drifters released at 150°W in May were around 3.6°N, 117°W in October, which is close to the position reached

by *in situ* drifters (3°N, 120°W). The remaining 7 drifters formed the southern group that was swept southward in July. In this group, the model reproduced the timing of the direction changes. While *in situ* drifters travelled 4 to 6 degrees further south in the vicinity of 160°W than virtual drifters, *in situ* and virtual drifters had about the same southward drift along 140°W. Further east, the 3 *in situ* buoys that started in the equatorial zone near 100°W remained in the eastern basin. In the model, part of the drifters released at 100°W meandered in the complex circulation patterns in the eastern part of the upwelling. The remaining part travelled south. These results suggest that the modeled southward velocity has been underestimated in the central western Pacific. However, measured and modeled meridional velocities during the fall 1997 are in agreement. Whereas the measured meridional component is greater than 0.1 m s^{-1} along 155°W south of 4°S and smaller further east, the modeled meridional component always ranges between 0 and 0.05 m s^{-1}. *In situ* drifters located in the southeast region (115°W-3°S and 90°W-9°S) show a westward component which is stronger than in the model, especially at the end of the period. *In situ* buoys released in May in the 12°S-13°S region had a strong westward drift that was not reproduced in the central basin by the model. The agreement was better in the western zone.

3.2 Nitrate and new production

In late 1996, before the onset of the event, the surface nitrate concentrations in the central Pacific were representative of cold conditions both in the observations (Strutton and Chavez 2000) and in the model (Fig. 4). However, the modeled nitrate was underestimated by 1.5 to 2 μM. The nitrate concentration fell abruptly near 2-4°N (convergence and downwelling zone, advection of low nitrate water from the west by the NECC) while the decrease at the southern edge of the upwelling was smoother. Modeled new production was within the range of values found in the literature. It was lower than 1 mmol N m^{-2} d^{-1} in the oligotrophic region whereas in the Wyrtki (1981) box (5°S-5°N; 90°W-180°) it was 1.9 mmol N m^{-2} d^{-1} which is slightly lower than values inferred from measurements or from other physical-biological coupled models. The model reproduced the relationship between measured nitrate concentrations integrated over the euphotic layer and new production as established by Raimbault et al. (1999) for the tropical Pacific. In particular, the rate of increase of new production in the HNLC region was very slow despite high nitrate concentration. Immediately following the strong westerly wind burst of March 1997, the warm pool started to move eastward. In the model, nitrate-poor waters reached 170°W in May and 155°W about one month later which

was consistent with the satellite-observed progression of chlorophyll-poor waters (Radenac et al. 2001; Ryan et al. 2002). As a result, nitrate disappeared along 170°W and the nitrate decrease along 155°W after December 1996 was about the same (40%) between 4°S and 4°N for the observations (Strutton and Chavez 2000) and for the model (Fig. 4). The insufficient nitrate decrease simulated around 2°N in May 1997 must be related to the weakness of the modeled NECC during that period. During the peak of the event, more than six months after the El Niño event started, nitrate and new production measured in the central equatorial Pacific were representative of warm pool conditions which were reproduced in the model. Conversely, the uplift of the nitracline in the western equatorial basin caused a relative increase of the chlorophyll concentration at the deep chlorophyll maximum and of new production (Turk et al. 2001; Radenac et al. 2001; Christian et al. 2002).

3.3 The Lagrangian analysis

3.3.1 Redistribution of water masses between May and December 1997

The distribution of surface water masses in May 1997 is shown in Fig. 5a. The nitrate-depleted layer of the warm pool was about 100 m deep between 160°E and 180°E close to the equator (Fig. 5b). It became thinner by 20 to 30 m poleward, in agreement with measurements (Mackey et al. 1995; Radenac and Rodier 1996; Turk et al. 2001). Farther north, the base of the nitrate-depleted layer of the northwest subtropical water was around 70 m and deepened north of 12°N as reported during cruises (Kaneko et al. 1998). For the central Pacific, the model reproduced the asymmetry in nitrate distribution of the north and south subtropical waters (Wyrtki and Kilonsky 1984; Raimbault et al. 1999; Dugdale et al. 2002). As a result, the nitrate-depleted layer of the south subtropical water (that reaches 150 m south of 10°S) was deeper than that of the northeast subtropical water (about 80 m). The nitracline of the upwelling equatorial waters shoaled eastward in agreement with the thermocline slope (Fig. 5b).

In order to find the origin of water masses for a given month, virtual water particles were released at each surface grid point of the model (5849 particles). They were tracked backward in the three-dimensional velocity field until May 1997, when water masses were defined. In this way, the release position for the selected month was associated with the water mass of origin. The redistribution of water masses since May was followed using such mapping performed for each month between June and December. Two intermediate phases of

this progression in July (Fig. 5c) and September (Fig. 5d) are shown as well as the peak phase in December (Fig. 5e). Less than 1% of drifters that reach the surface in July, September, or December come from subsurface waters. It should be noted, however, that drifters at the surface in July, September, or December may come from relatively deep within the body of surface water masses.

The main displacements in the surface layer between May and December concerned the oligotrophic warm pool (WPW) and northwest subtropical waters (NWSW) and the nitrate-rich upwelled water (UPW) (Fig. 5). During a first phase (May-July), oligotrophic water from the northwest tropical Pacific expanded southwards in the western basin while water from the warm pool spread eastward (30° along the equator), breaking through the upwelling water (Fig. 5c). In July-August, waters from the northwest had reached the equator and began an eastward displacement. Meanwhile, following a brief episode of westward flow, the upwelling waters shifted westward and separated oligotrophic waters into two branches, leading to the September situation (Fig. 5d). During the following months, oligotrophic waters again spread eastward, with the northern branch progressing a little bit faster than the southern branch. The south-eastward intrusion of northwest tropical water toward the central basin in fall 1997 was consistent with the freshening observed in late 1997 in this region (Johnson et al. 2000). In December (Fig. 5e), a northeast-southwest oriented line (between 8°N-120°W and 10°S-140°W) marked the easternmost expansion of warm pool and northwest subtropical waters. In the south, the eastern limit of south subtropical waters was oriented northwest-southeast. Waters that originated in the upwelling were located to the east of these boundaries.

The leading edge of eastward spreading 'pre El Niño' oligotrophic waters did not match the limit of the nitrate rich surface waters ($NO_3 > 1$ μM) of the December dwindling upwelling (Fig. 5e). Actually, this simple diagram suggests that the main surface water masses redistributed according to three schemes during the 1997 El Niño. First, advection without transformation prevailed west of the oligotrophic invasion boundary: oligotrophic waters from the western and northwestern tropical Pacific spread toward the central basin with minor nitrate changes. Second, the region inside the nitrate-rich December 1997 limit was a retention zone where drifters have complex trajectories within the upwelled water mass as observed with *in situ* drifters (Fig. 3). Third, east of the leading edge and outside the remaining upwelling (delimited by the 1 μM isoline), nitrate had been exhausted during the drift of water masses that were originally nitrate-rich: advection together with transformation predominated. In that case, water masses followed two main paths. (1) North of the December residual upwelling, drifters came essentially from the western part of the May upwelling

waters. They were caught in the strong NECC flow and moved eastward toward the Gulf of Panama. (2) South of the December upwelling, drifters originally in the upwelling region followed the southward surface circulation that develops during the fall in the central basin (Fig. 3). Both pathways have been observed with *in situ* drifters (Fig. 3).

3.3.2 Lagrangian nitrate changes

Fig. 6 is an example of nitrate transformations that take place along trajectories according to the advection/transformation scheme during the May-December 1997 period. These nitrate changes are the consequence of mixing with the neighboring water masses and biological effect (Eq. 3). In order to investigate those transformations, properties such as depth, nitrate concentration, horizontal and vertical diffusion and biological effect are sampled along the trajectories of drifters released at the surface in the western part of the upwelling in early May (along 150°W between 2°S and 2°N).

Within one month, drifters split into the north and south groups as previously mentioned (Fig. 6a). Their behavior was quite similar. Drifters remained in the upper 20 m, except for drifters of the northern group that deepened to about 40 m at the end of the period (Fig. 6b and 6c). It takes about 120 days for drifters released in waters with nitrate concentrations of about 2.5 μM to become depleted (Fig. 6b and 6c). In May 1997 and during the depletion period, vertical nitrate supply in the central and eastern equatorial Pacific had greatly decreased (Chavez et al. 1999; Radenac et al. 2001; Christian et al. 2002). As expected, the lateral and vertical nitrate diffusions remained small along the drift of particles and nitrate changes along trajectories were essentially driven by the biological uptake between May and September (Fig. 6d and 6e). Along the northern pathway (Fig. 6d), the nitrate-impoverished drifters reached the NECC flow in September and accumulated in the direction of the Gulf of Panama. During their eastward drift north of the upwelling, the horizontal diffusion balanced the nitrate uptake and the nitrate concentration stayed close to zero. Along the southern pathway (Fig. 6e), nitrate was assimilated by phytoplankton while the particles drifted slowly. After September, nitrate was definitely exhausted, giving these waters the same properties as oligotrophic waters of the subtropical south Pacific. For both drifter groups, biology drove the nitrate depletion during this period with dynamical characteristics specific of a mature El Niño phase.

Fig. 7 shows a generalization of this experiment over the tropical Pacific basin. Drifters were released in December in the surface layer at each grid point of the model and

then tracked backward until May. For each trajectory, the nitrate consumption between May and December (ΔNO_3) was computed and the biological (bio) and diffusion (phy) effects integrated. In order to compare the order of magnitude of those quantities in December, –phy is presented in Fig. 7c (i.e. nitrate gain is negative). As expected in the region west of the limit of eastward spreading oligotrophic waters, advection of poor water prevailed and no major nitrate changes occurred (Fig. 7a). East of this limit, nitrate diminished. Drifters that had reached the eastern part of the NECC or that were situated southward of the upwelling in December had lost 2 to 5 μM nitrate. The nitrate fall could be even higher within the upwelling region. Some sparse small spots of nitrate increase were found in the upwelling and off the Central American coast. The physical inputs integrated over the May-December period were negligible west of the leading edge of eastward spreading oligotrophic waters. East of the limit, the surface circulation patterns that had drastically changed at the onset of the event only resulted in small physical inputs. The biological response was slower and during that period, nitrate assimilation remained rather stable. As a result, the biological consumption was greater than the physical inputs and drove the nitrate impoverishment.

4 Discussion

The reliability of the GCM is an essential point for this study. There was general agreement between modeled and observed surface circulation for 1997, in spite of a slight local underestimation of the meridional velocity. The model accurately reproduced the timing of the reversals of current at the equator. In particular, the strong eastward flow in May-June and the brief SEC return in July-August were well captured. Imperfections in the mixing scheme caused the thermocline and therefore the nitracline, to be too diffusive (Vialard et al. 2001; Radenac et al. 2001; Lengaigne et al. 2003). Consequently, the nitrate flux into the modeled surface mixed layer should be too high. This bias caused a very strong new primary production during the first years of the spin-up phase that was initially performed for the nitrate field to reach equilibrium with the large-scale dynamics (Radenac et al. 2001). The overall effect of abnormally high diffusion during the spin-up (8 years) was to transfer too much nitrate from just below the pycnocline into the mixed layer and then to immediately export it at depth, exponentially. Finally, this led to abnormally low nitrate concentrations in the lower part of the nitracline whereas the modeled nitrate values remained consistent with observations in the mixed layer.

The constants V_{max} and K_{NO3} in the biogeochemical model had been estimated in order to reproduce as faithfully as possible the nitrate concentrations observed in the photic layer (Stoens et al., 1999). The model is based on the common assumption that nitrate fixation equals new and exported production. Vmax was in the range of values found after field experiments (Stoens et al. 1999). On the contrary, K_{NO3} = 0.01 μM was much lower than values generally admitted. This biologically unrealistic value had to be adopted to balance the excessive nitrate diffusion flux into the mixed layer in the oligotrophic warm pool waters. Higher K_{NO3} values indeed led to slow nitrate assimilation when nitrate concentration was low, so that nitrate was always present in the warm pool photic layer instead of being totally depleted, as it really is. This choice had no consequences in upwelled waters with significant amounts of nitrate, where nitrate assimilation is in fact driven by V_{max}. Since these constants finally reproduced the nitrate variability in the main oligotrophic and mesotrophic regions and the slow nitrate uptake of the HNLC ecosystem, it was considered that the modeled nitrate assimilation does not largely differ from the actual nitrate fixation. These considerations only concern the oligotrophic and HNLC water masses prior to and during the 1997-98 El Niño. They should not apply to the recovery phase immediately after this event, when upwelling resumed and brought nitrate-rich waters and iron from below into an entirely oligotrophic ocean in which grazers populations were at their lowest level (Murtugudde et al. 1999; Ryan et al. 2002).

In order to understand how the evolution of nitrate-poor and nitrate-rich surface waters led to the biological situation as seen by ocean color during the peak of the 1997 El Niño event, the trajectories of drifters which were simply released in the first layer of the model were analyzed. Although the chlorophyll concentration estimated from ocean color data is approximately the mean chlorophyll concentration between the surface and the first attenuation length, a large part of the ocean color signal can be explained by the pigment concentration of the upper 10 m layer. The first attenuation length varies as the inverse of the attenuation coefficient K_d, at the 490 nm wavelength used in the SeaWiFS algorithm (Morel and Maritorena 2001). Therefore, if we exclude coastal waters, it is about 40 m in oligotrophic waters where chlorophyll is lower than 0.1 mg m^{-3} and about 30 m in waters with chlorophyll ranging between 0.1 and 0.3 mg m^{-3}. In the first case, the upper 2 layers of the model (0-20 m) would account for more than 60% of the signal while in the second case, the first layer alone would account for about 50%. Besides, during the singular period studied, drifters released in the surface layer remained within the mixed layer. Part of the drifters released in May in the western part of the upwelling was caught in the NECC and drifted near

the surface toward the Gulf of Panama (Fig. 6b). The reverse experiment strengthened this result: 54% of the virtual drifters released in December 1997 in the eastern part of the NECC (247 parcels released between 3°N and 6°N and between 115°W and the American coast) originated from the surface HNLC waters of the western part of the equatorial divergence. Virtual drifters that reached south of the upwelling in December surfaced at the equator before or at the beginning of the period and then drifted southward near the surface. Consequently, because a large part of the ocean color signal may be explained by the pigment concentration of the upper 10 m layer and because drifters remained in the mixed layer during the El Niño period, the conclusion of the study as to the origin of water masses of the first layer of the model is reasonable.

5 Conclusion

This study contributes to the general issue of the relative contributions of physical and biological processes to the setting of El Niño oligotrophic conditions. Because chlorophyll is often used as a proxy for phytoplankton biomass, ocean color imagery is a key instrument for monitoring the relative extension of phytoplankton rich and poor waters at different timescales. They may be hints we can grasp about the underlying mechanisms by observing surface chlorophyll patterns and their evolution. However, there was a gap in sea color coverage between June and September 1997, i. e. when most of the pre-El Niño surface layer nitrate was being consumed (Fig. 6). A deeper insight of these processes is possible using numerical simulations, although they do not perfectly reproduce the real ocean. A Lagrangian analysis applied to the output of a coupled physical-biogeochemical model shows that surface nitrate-rich and nitrate-poor water masses redistributed following three schemes during the 1997 El Niño. First, oligotrophic waters from the western Pacific remained oligotrophic during the course of their eastward transport. This mechanism is the most documented one along the equator (Chavez et al. 1998; Stoens et al. 1999; Strutton and Chavez 2000; Radenac et al. 2001; Christian et al. 2002) and highlights the impact that variability of the general circulation may have on the biological variability at a first order. Second, an upwelling system persists in the eastern part of the basin. This study emphasized a third scheme that represents an alternative to generalized nitrate-poor water conditions. During El Niño events, lateral and vertical nitrate inputs are greatly reduced in the HNLC region because of the equatorial deepening of the nutricline (Chavez et al. 1998; Stoens et al. 1999; Strutton and Chavez 2000; Radenac et al. 2001; Christian et al. 2002) and the decrease in activity of the tropical

instability waves (Philander et al. 1985). The biological uptake then becomes the main process that drives the nitrate depletion along trajectories and, as a consequence, the 'new' oligotrophic regions form a continuous stripe that surrounds the HNLC zone during a mature El Niño phase. Because of the slow nitrate uptake characteristic of the tropical Pacific HNLC system, nitrate that was present in the euphotic layer at the early stage of El Niño was able to sustain a biological production during several months. Thus, the slow nitrate uptake characteristic of HNLC waters delayed the onset of poor conditions.

Other studies have shown that in several regions of the tropical Pacific, the biological response to El Niño is opposed to that of the HNLC zone. In the western Pacific, the basin tilt of the thermocline and nutricline resulted in higher nitrate content in the euphotic layer and increased biological activity as shown by Radenac et al. (2001), Turk et al. (2001), or Christian et al. (2002) for the 1997 event. Similar vertical processes lead to the north equatorial enrichment that has been reported during several El Niño events. Abnormally high chlorophyll concentration was measured during the second half of the 1982-1983 El Niño in a wide area centered in the warm pool at 170°E, 10°N (Dandonneau 1992); at the same time, Dymond and Collier (1988) measured stronger biogenic particle fluxes at 140°W, 11°N than during non-El Niño years; in 1997, the SeaWiFS imagery revealed a large zone of surface chlorophyll higher than 0.1 mg m^{-3} that extended from about 10°N off the central American coast southwestward toward the equator (Murtugudde et al. 1999).

The idea that the tropical Pacific is a biological desert during El Niño years relies mainly on equatorial studies. The above-mentioned observations of increased biological activity off the equator together with this investigation suggest that our usual view of the biological consequences of El Niño in the tropical Pacific should be tempered.

Acknowledgements We would like to thank G. C. Johnson, F. Bonjean and G. Lagerloef for providing the ADCP cruise data and the satellite-derived currents. Out thanks as well to the Drifter Data Assembly Center, GOOS Center, NOAA/AOML, Miami, Florida, for their quality control of the drifter data and for making it available through the web. J. Sudre extracted the ocean color data. Special thanks to C. Maes and F. Melin and to two anonymous reviewers for constructive comments.

References

Barber RT, Chavez FP (1983) Biological consequences of El Niño. Science 222: 1203-1210

Bender ML, McPhaden MJ (1990) Anomalous nutrient distribution in the equatorial Pacific in April 1988: evidence for rapid biological uptake. Deep-Sea Res 37: 1075-1084

Blanke B, Raynaud S (1997) Kinematics of the Pacific equatorial undercurrent: an eulerian and Lagrangian approach from GCM results. J Phy Oceanogr 27: 1038-1053

Bonjean F, Lagerloef GSE (2002) Diagnostic model and analysis of the surface currents in the tropical Pacific Ocean. J Phy Oceanogr 32(10): 2938-2954

Boutin J, Etcheto J, Dandonneau Y, Bakker DCE, Feely RA, Inoue HY, Ishii M, Ling RD, Nightingale PD, Metzl N, Wanninkhof R (1999) Satellite sea surface temperature: A powerful tool for interpreting in situ pCO_2 measurements in the equatorial Pacific ocean. Tellus 51(B): 490-508

Chavez FP, Strutton PG, McPhaden MJ (1998) Biological-physical coupling in the central Pacific during the onset of the 1997-98 El Niño. Geophys Res Lett 25(19): 3543-3546

Chavez FP, Strutton PG, Friederich GE, Feely RA, Feldman GC, Foley DG, McPhaden MJ (1999) Biological and chemical response of the equatorial Pacific Ocean to the 1997-98 El Niño. Science 286: 2126-2131

Christian JR, Verschell MA, Murtugudde R, Busalacchi AJ, McClain CR (2002) Biogeochemical modelling of the tropical Pacific ocean. I. Seasonal and interannual variability. Deep-Sea Res II 49: 509-543

Coale KH, Fitzwater SE, Gordon RM, Johnson KS, Barber RT (1996) Control of community growth and export production by upwelled iron the equatorial Pacific Ocean. Nature 379: 621-624

Dandonneau Y (1979) Concentrations en chlorophylle dans le Pacifique tropical sud-ouest: comparaison avec d'autres aires océaniques tropicales. Oceanol Acta 2: 133-142

Dandonneau Y, Eldin G (1987) Southwestward extent of chlorophyll-enriched waters from the Peruvian and equatorial upwellings between Tahiti and Panama. Mar Ecol Progr Ser 38: 283-294

Dandonneau Y (1992) Surface chlorophyll concentration in the Tropical Pacific Ocean: an analysis of data collected by merchant ships from 1978 to 1989. J Geophys Res 97: 3581-3591

Deschamps PY, Breon FM, Leroy M, Podaire A, Bricaud A, Buriez JC, Seze G (1994) The POLDER Mission: Instrument Characteristics and Scientific Objectives. IEEE Trans Geoscience Remote Sensing 32: 598-615

Dugdale RC, Barber RT, Chai F, Peng TH, Wilkerson FP (2002) One-dimensional ecosystem model of the equatorial Pacific upwelling system. Part II: sensitivity analysis and comparison with JGOFS EqPac data. Deep-Sea Res II 49: 2747-2768

Dymond J, Collier R (1988) Biogenic particle fluxes in the equatorial Pacific: evidence for both high and low productivity during the 1982-1983 El Niño. Global Biogeoch Cycles 2(2): 129-137

Eldin G, Rodier M, Radenac MH (1997) Physical and nutrient variability in the upper equatorial Pacific associated with westerly wind forcing and wave activity in October 1994. Deep-Sea Res II 44: 1783-1800

Friedrichs MAM, Hofmann EE (2001) Physical control of biological processes in the central equatorial Pacific Ocean. Deep-Sea Res I 48: 1023-1069

Hansen DV, Poulain PM (1996) Quality control and interpolations of WOCE/TOGA drifter data. J Atmosph Oceanic Technol 13: 900-909

Hardy J, Hanneman A, Behrenfeld M, Horner R (1996) Environmental biogeography of near-surface phytoplankton in the southeast Pacific Ocean. Deep-Sea Res I 43(10): 1647-1659

Hayes SP, Chang P, McPhaden MJ (1991) Variability of the sea surface temperature in the eastern equatorial Pacific during 1986-88. J Geophys Res 96: 10553-10566

Honjo S (1978) Sedimentation of material in the Sargasso Sea at 5,367 m. J Mar Res 36: 469-492

Inoue HY, Ishii M, Matsueda H, Ahoyama M (1996) Changes in longitudinal distribution of the partial pressure of CO_2 (pCO_2) in the central and western equatorial Pacific, west of 160°W. Geophys Res Lett 14: 1781-1784

Johnson GC, McPhaden MJ, Rowe GD, McTaggart KE (2000) Upper equatorial Pacific Ocean current and salinity variability during the 1996-1998 El Niño-La Niña cycle. J Geophys Res 105: 1037-1053

Kaneko I, Takatsuki Y, Kamiya H, Kawae S (1998) Water property and current distributions along the WHP-P9 section (137°-142°E) in the western North Pacific. J Geophys Res 103(C6): 12959-12984

Karl DM, Lukas R (1996) The Hawaii Ocean Time-series (HOT) program: Background, rationale and field implementation. Deep-Sea Res II 43(2-3): 129-156

Kobayashi F, Takahashi K (2002) Distribution of diatoms along the equatorial transect in the western and central Pacific during the 1999 La Niña conditions. Deep-Sea Res II 49: 2801-2821

Kuroda Y, McPhaden MJ (1993) Variability in the western equatorial Pacific Ocean during Japanese Pacific Climate Study Cruises in 1989 and 1990. J Geophys Res 98: 4747-4759

Lagerloef GSE, Mitchum GT, Lukas RB, Niiler PP (1999) Tropical Pacific near-surface currents estimated from altimeter, wind, and drifter data. J Geophys Res 104: 23313-23326

Landry MR, Barber RT, Bidigare RR, Chai F, Coale KH, Dam HG, Lewis MR, Lindley ST, McCarthy JJ, Roman MR, Stoecker DK, Verity PG, White JR (1997) Iron and grazing constraints on primary production in the central equatorial Pacific: An EqPac synthesis. Limnol Oceanogr 42: 405-418

Le Borgne R, Barber RT, Delcroix T, Inoue HY, Mackey DJ, Rodier M (2002) Pacific warm pool and divergence: temporal and zonal variations on the equator and their effects on the biological pump. Deep-Sea Res II 49: 2471-2512

Lehodey P, André JM, Bertignac M, Hampton J, Stoens A, Menkes C, Memery L, Grima N (1998) Predicting skipjack tuna forage distributions in the equatorial Pacific using a coupled dynamical bio-geochemical model. Fish Oceanogr 7: 317-325

Lengaigne M, Madec G, Menkes C, Alory G (2003) Impact of isopycnal mixing on the tropical ocean circulation. J Geophys Res 108(C11) DOI:10.1029/2002JC001704

Mackey DJ, Parslow J, Higgins HW, Griffiths FB, O'Sullivan JE (1995) Plankton productivity and biomass in the western equatorial Pacific: biological and physical controls. Deep-Sea Res II 42: 499-533

Maes C, Madec G, Delecluse P (1997) Sensitivity of an equatorial Pacific OGCM to the lateral diffusion. Mon Wea Rev 125: 958-971

McClain CR, Cleave ML, Feldman GC, Gregg WW, Hooker SB, Kuring N (1998) Science quality SeaWiFS data for global biosphere research. Sea Technol 39: 10-16

McPhaden MJ, Picaut J (1990) El Niño-Southern Oscillation displacements of the western equatorial Pacific warm pool. Science 250: 1385-1388

McPhaden MJ, Busalacchi AJ, Cheney R, Donguy JR, Gage KS, Halpern D, Ji M, Julian P, Meyers G, Mitchum GT, Niiler PP, Picaut J, Reynolds RW, Smith N, Takeuchi K (1998) The Tropical Ocean-Global Atmosphere observing system: A decade of progress. J Geophys Res 103: 14169-14240

Morel A, Maritorena S (2001) Bio-optical properties of oceanic waters: A reappraisal. J Geophys Res 106: 7163-7180

Murakami H, Ishizaka J, Kawamura H (2000) ADEOS observations of chlorophyll a concentration, sea surface temperature, and wind stress change in the equatorial Pacific during the 1997 El Niño onset. J Geophys Res 105: 19551-19559

Murtuggude RG, Signorini SR, Christian JR, Busalacchi AJ, McClain CR, Picaut J (1999) Ocean color variability of the tropical Indo-Pacific basin observed by SeaWiFS during 1997-98. J Geophys Res 104: 18351-18365

Navarette C (1998) Dynamique du phytoplancton en océan équatorial: mesures cytométriques et mesures isotopiques durant la campagne FLUPAC, en octobre 1994 dans la partie ouest du Pacifique. Thèse de Doctorat de l'Université Paris VI

Niiler P (2001) The world ocean surface circulation. In: Church J, Siedler G, Gould J (eds) Ocean Circulation and Climate-Observing and Modeling the Global Ocean, Academic Press, pp 193-204

Pazan SE, Niiler P (2004) New global drifter data set available. EOS, Trans Amer Geophys Union, 85(2)

Philander SGH, Halpern D, Hansen D, Legeckis R, Miller L, Paul C, Watts R, Weisberg R, Winbush M (1985) Long waves in the equatorial Pacific Ocean. EOS, Trans Amer Geophys Union, 66: 154.

Picaut J, Ioualalen M, Menkes C, Delcroix T, McPhaden MJ (1996) Mechanisms of the zonal displacements of the Pacific warm pool: implications for ENSO. Science 274: 1486-1489

Price NM, Ahner BA, Morel FMM (1994) The equatorial Pacific Ocean: grazer-controlled phytoplankton populations in an iron-limited ecosystem. Limnol Oceanogr 39(3): 520-534

Radenac MH, Rodier M (1996) Nitrate and chlorophyll distributions in relation to thermohaline and current structures in the western tropical Pacific during 1985-1989. Deep-Sea Res II 43: 725-752

Radenac MH, Menkes C, Vialard J, Moulin C, Dandonneau Y, Delcroix T, Dupouy C, Stoens A, Deschamps PY (2001) Modeled and observed impacts of the 1997-1998 El Niño on nitrate and new production in the equatorial Pacific. J Geophys Res 106: 26879-26898

Raimbault P, Slawyk G, Boudjellal B, Coatanoan C, Conan P, Coste B, Garcia N, Moutin T, Pujo-Pay M (1999) Carbon and nitrogen uptake and export in the equatorial Pacific at 150°W: Evidence of an efficient regenerated production cycle. J Geophys Res 104: 3341-3356

Reverdin G, Frankignoul C, Kestenare E, McPhaden MJ (1994) Seasonal variability in the surface currents of the equatorial Pacific. J Geophys Res 99: 20323-20344

Reynolds RW, Smith TM (1994) Improved global sea surface temperature analyses using optimum interpolation. J Clim 7: 929-948

Ryan JP, Polito PS, Strutton PG, Chavez FP (2002) Unusual large-scale phytoplankton blooms in the equatorial Pacific. Progr Oceanogr 55(3): 263-285

Stoens A, Menkes C, Radenac MH, Grima N, Dandonneau Y, Eldin G, Memery L, Navarette C, André JM, Moutin T, Raimbault P (1999) The coupled physical-new production system in the equatorial Pacific during the 1992-1995 El Niño. J Geophys Res 104: 3323-3339

Strutton PG, Chavez FP (2000) Primary productivity in the equatorial Pacific during the 1997-98 El Niño. J Geophys Res 105: 26089-26101

Turk D, Lewis MR, Harrison GW, Kawano T, Asanuma I (2001) Geographical distribution of new production in the western/central equatorial Pacific during El Niño and non-El Niño conditions. J Geophys Res 106: 4501-4515

Vialard J, Menkes C, Boulanger JP, Delecluse P, Guilyardi E, McPhaden MJ, Madec G (2001) A model study of oceanic mechanisms affecting equatorial Pacific sea surface temperature during the 1997-98 El Niño. J Phy Oceanogr 31: 1649-1675

Vialard J, Delecluse P, Menkes C (2002) A modeling study of salinity variability and its effects in the tropical Pacific ocean during the 1993-99 period. J Geophys Res 107(C12) DOI:10.1029/2000JC000758

Wyrtki K (1981) An estimate of equatorial upwelling in the Pacific. J Phy Oceanogr 11: 1205-1214

Wyrtki K, Kilonsky B (1984) Mean water and current structure during the Hawaii to Tahiti shuttle experiment. J Phy Oceanogr 14: 242-254

Fig. 1a-c Modeled surface velocity (vectors, m s^{-1}) superimposed on satellite chlorophyll (color scale, mg m^{-3}). The November 1996 (**a**) and May 1997 (**b**) scenes are POLDER derived chlorophyll, the December 1997 panel (**c**) is SeaWiFS chlorophyll. The *white full line* corresponds to 0.1 mg m^{-3}. The *white dashed line* in December is the leading edge of eastward spreading 'pre El Niño' oligotrophic waters.

Fig. 2a-c Zonal velocity component (m s^{-1}) along 155°W between November 1996 and December 1997. **a** Time evolution of the satellite-derived surface zonal current (OSCAR). **b** Time evolution of the modeled zonal current at 15 m. The contour interval is 0.25 m s^{-1}. Positive values are shaded. The vertical lines represent the December 1996, May 1997 and November 1997 cruises. **c** Meridional profiles of ADCP zonal current measured at 15 m during cruises along 155°W in December 1996 (*small-dashed line*), May 1997 (*solid line*) and November 1997 (*long-dashed line*).

Fig. 3a-b Comparison of (**a**) *in situ* drifters and (**b**) modeled trajectories between May and December 1997. Colors are one-month intervals between the beginning (May) and the end (December) of trajectories.

Fig. 4 Meridional distributions of measured (top panels; adapted from Strutton and Chavez 2000) and modeled (bottom panels) surface nitrate before (late 1996; left panels) and during (May 1997; right panels) El Niño along 155°W (*triangle*) and 170°W (*circle*).

Fig. 5a-e Redistribution of surface water masses between May and December 1997. **a, b** Surface distribution of water masses of origin and their vertical section along the equator in May 1997. **c, d, e** Origin of water masses in July, September and December 1997. The color key represents water masses: warm pool water (WPW), north-west subtropical water (NWSW), north-east subtropical water (NESW), south subtropical water (SSW), equatorial upwelling water (UPW), subsurface water (SUBS). Remaining cases, essentially coastal upwelling waters, are mentioned in black. The *thick black line* is the 1 μM surface nitrate concentration at the time of the release. The *dashed line* in December is the leading edge of eastward spreading 'pre El Niño' oligotrophic waters. The model grid causes the horizontal stripes.

Fig. 6a-e Results of the direct experiment: drifters are released at 150°W in May 1997 and reach their end point in December 1997. **a** Evolution of the nitrate concentration (μM; color key) along the trajectories. **b** Time-series of the mean depth (m; *full line*) and NO_3 concentration (μM; *dashed line*) along the northern pathway. **c** Time-series of the mean depth and NO_3 concentration along the southern pathway. **d** Time-series of the horizontal diffusion (*blue line*), vertical diffusion (*red line*) and biological uptake (*green line*) in μmole NO_3 m^{-3} d^{-1} along the northern pathway. **e** Time-series of the horizontal diffusion, vertical diffusion and biological uptake along the southern pathway.

Fig. 7a-c Maps of the (**a**) NO_3 consumption and impacts of the (**b**) biological and (**c**) physical effects (μM; color key) between May and December 1997. The 1 μM surface nitrate isoline (*thick line*) is superimposed. The *dashed line* is the leading edge of eastward spreading 'pre El Niño' oligotrophic waters.

Table 1 Criteria used to define water masses in May 1997: 4 classes of oligotrophic water with $NO_3 < 1$ μM and 3 classes of nitrate-rich waters.

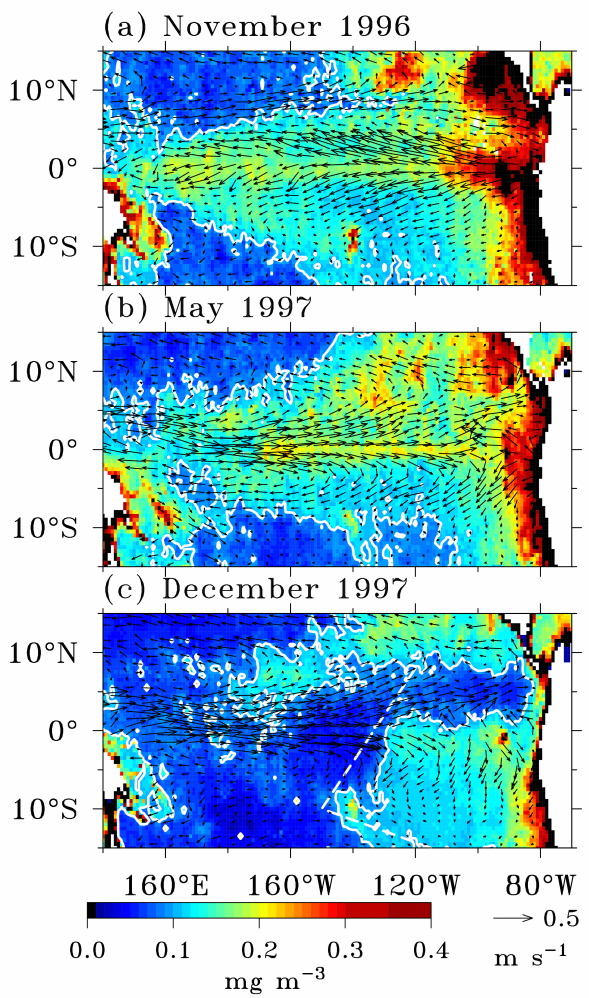

Fig. 1a-c Modeled surface velocity (vectors, m s^{-1}) superimposed on satellite chlorophyll (color scale, mg m^{-3}). The November 1996 (**a**) and May 1997 (**b**) scenes are POLDER derived chlorophyll, the December 1997 panel (**c**) is SeaWiFS chlorophyll. The *white full line* corresponds to 0.1 mg m^{-3}. The *white dashed line* in December is the leading edge of eastward spreading 'pre El Niño' oligotrophic waters.

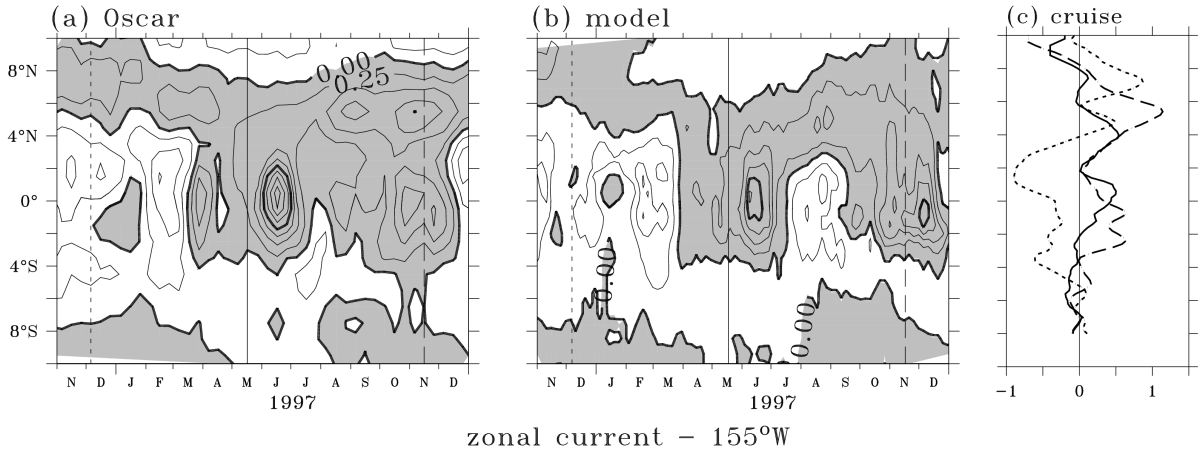

Fig. 2a-c Zonal velocity component (m s^{-1}) along 155°W between November 1996 and December 1997. **a** Time evolution of the satellite-derived surface zonal current (OSCAR). **b** Time evolution of the modeled zonal current at 15 m. The contour interval is 0.25 m s^{-1}. Positive values are shaded. The vertical lines represent the December 1996, May 1997 and November 1997 cruises. **c** Meridional profiles of ADCP zonal current measured at 15 m during cruises along 155°W in December 1996 (*small-dashed line*), May 1997 (*solid line*) and November 1997 (*long-dashed line*).

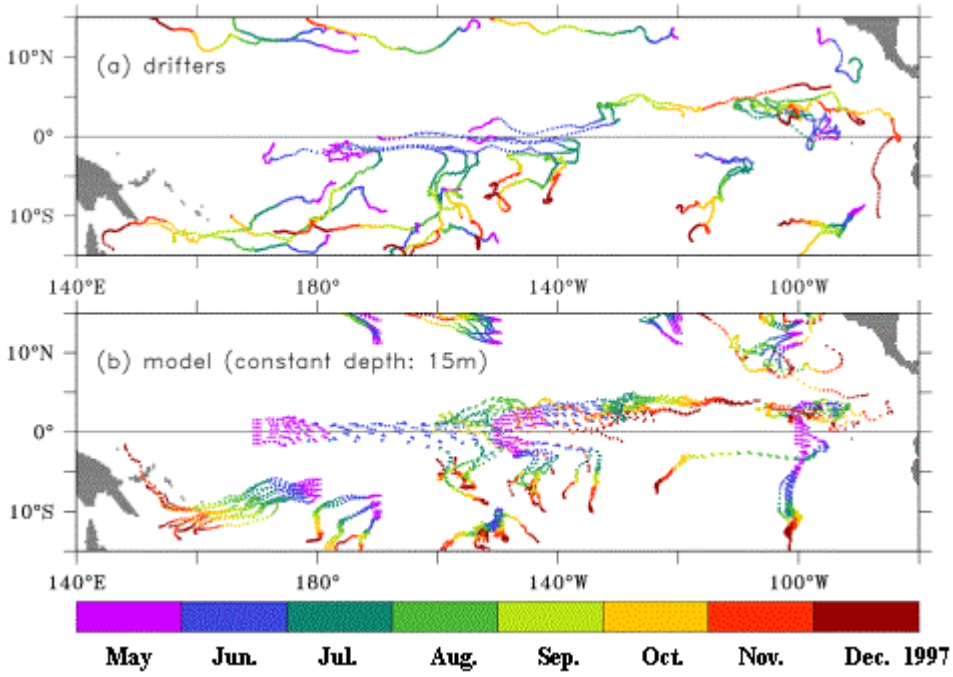

Fig. 3a-b Comparison of (**a**) *in situ* drifters and (**b**) modeled trajectories between May and December 1997. Colors are one-month intervals between the beginning (May) and the end (December) of trajectories.

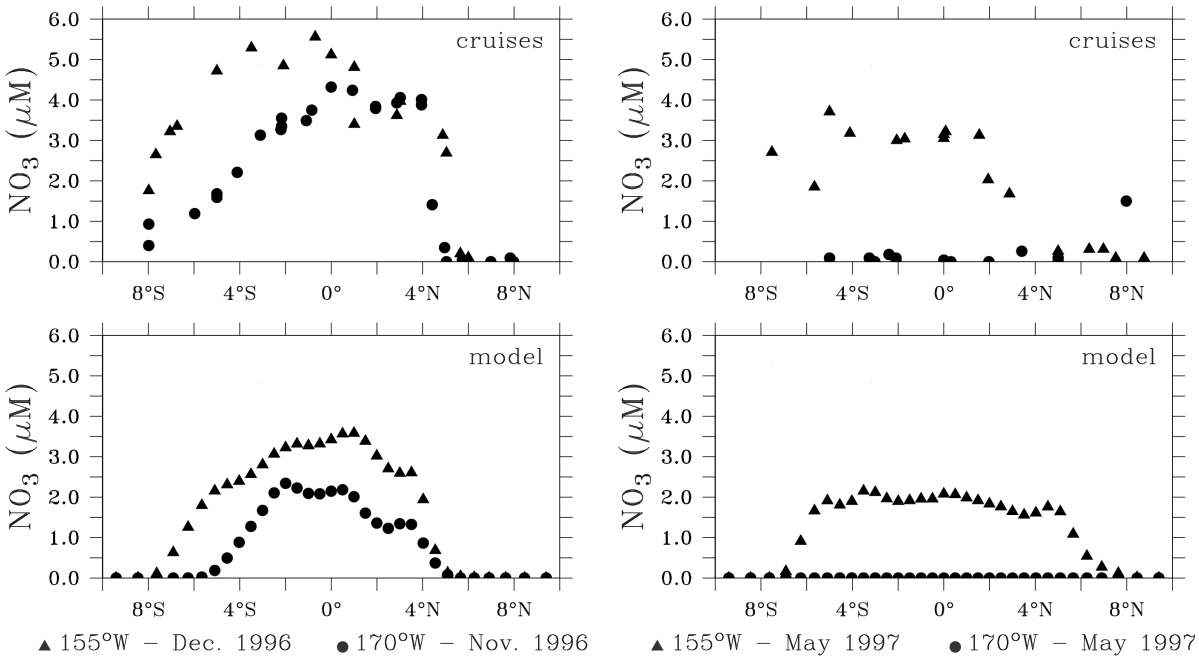

Fig. 4 Meridional distributions of measured (top panels; adapted from Strutton and Chavez 2000) and modeled (bottom panels) surface nitrate before (late 1996; left panels) and during (May 1997; right panels) El Niño along 155°W (*triangle*) and 170°W (*circle*).

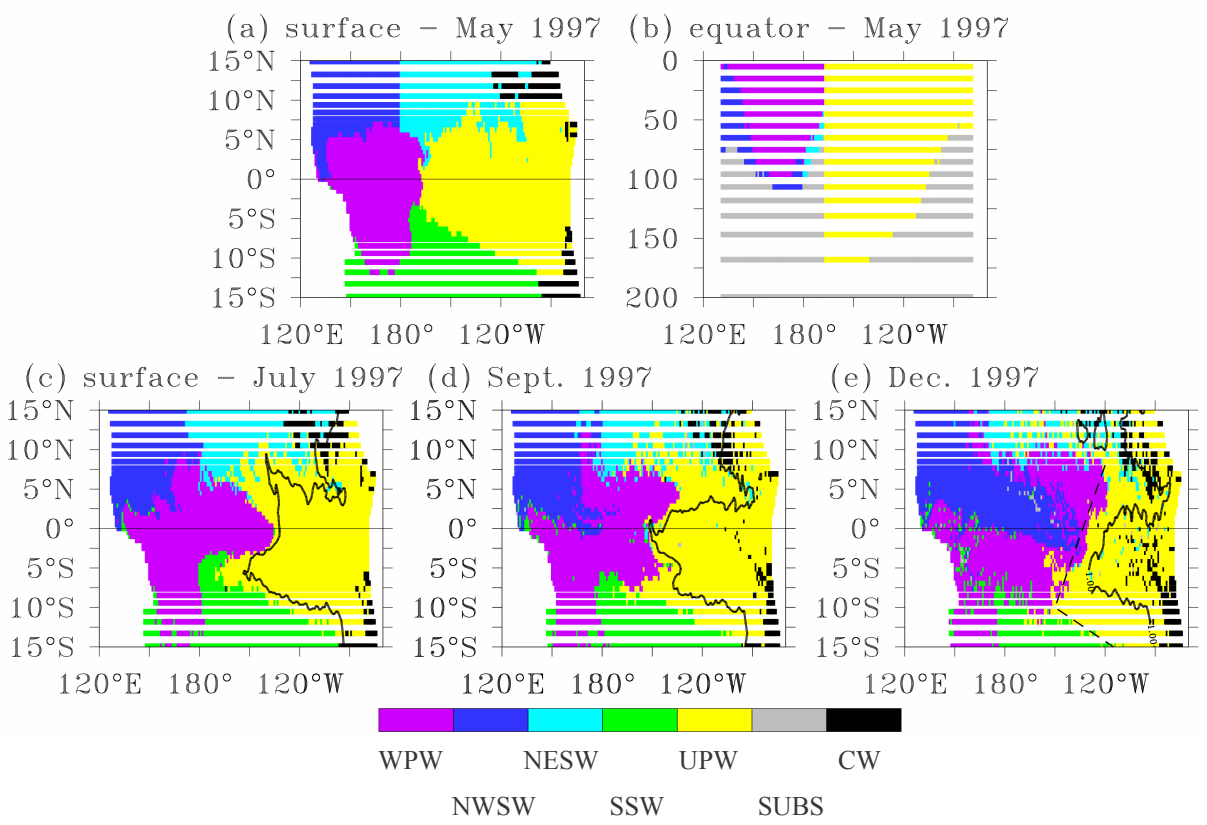

Fig. 5a-e Redistribution of surface water masses between May and December 1997. **a, b** Surface distribution of water masses of origin and their vertical section along the equator in May 1997. **c, d, e** Origin of water masses in July, September and December 1997. The color key represents water masses: warm pool water (WPW), north-west subtropical water (NWSW), north-east subtropical water (NESW), south subtropical water (SSW), equatorial upwelling water (UPW), subsurface water (SUBS). Remaining cases, essentially coastal upwelling waters, are mentioned in black. The *thick black line* is the 1 µM surface nitrate concentration at the time of the release. The *dashed line* in December is the leading edge of eastward spreading 'pre El Niño' oligotrophic waters. The model grid causes the horizontal stripes.

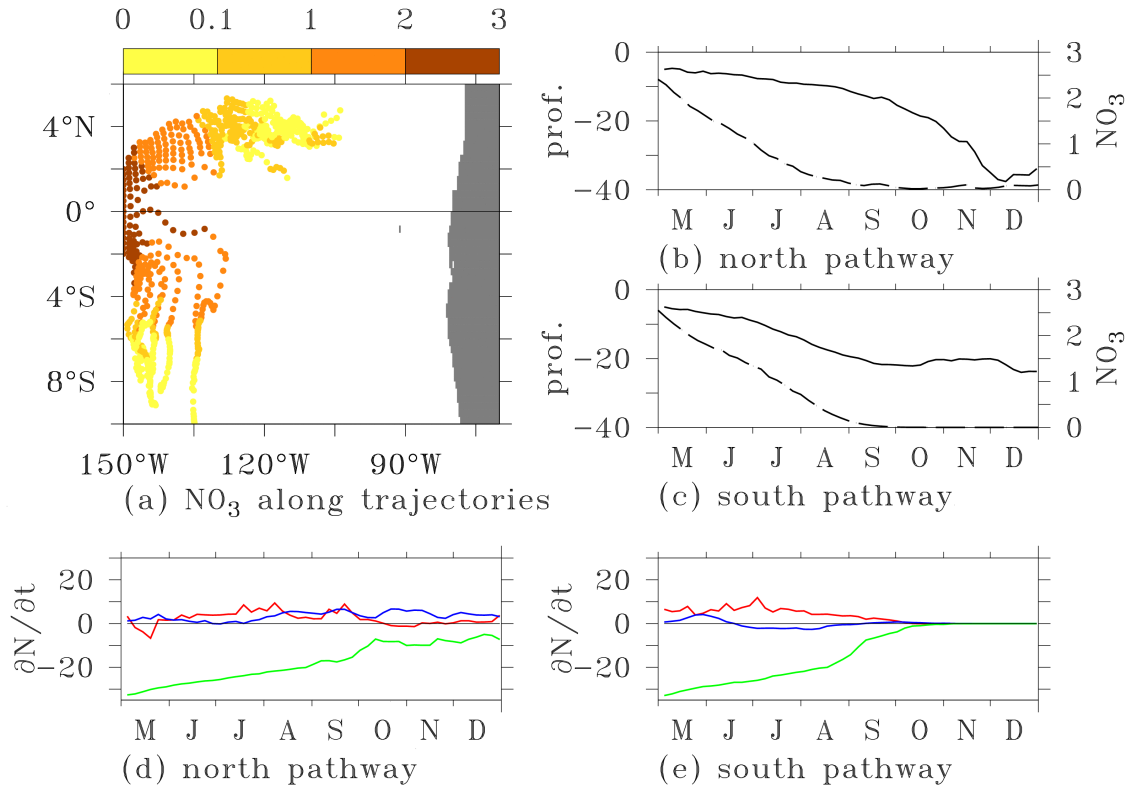

Fig. 6a-e Results of the direct experiment: drifters are released at 150°W in May 1997 and reach their end point in December 1997. **a** Evolution of the nitrate concentration (µM; color key) along the trajectories. **b** Time-series of the mean depth (m; *full line*) and NO_3 concentration (µM; *dashed line*) along the northern pathway. **c** Time-series of the mean depth and NO_3 concentration along the southern pathway. **d** Time-series of the horizontal diffusion (*blue line*), vertical diffusion (*red line*) and biological uptake (*green line*) in µmole NO_3 m^{-3} d^{-1} along the northern pathway. **e** Time-series of the horizontal diffusion, vertical diffusion and biological uptake along the southern pathway.

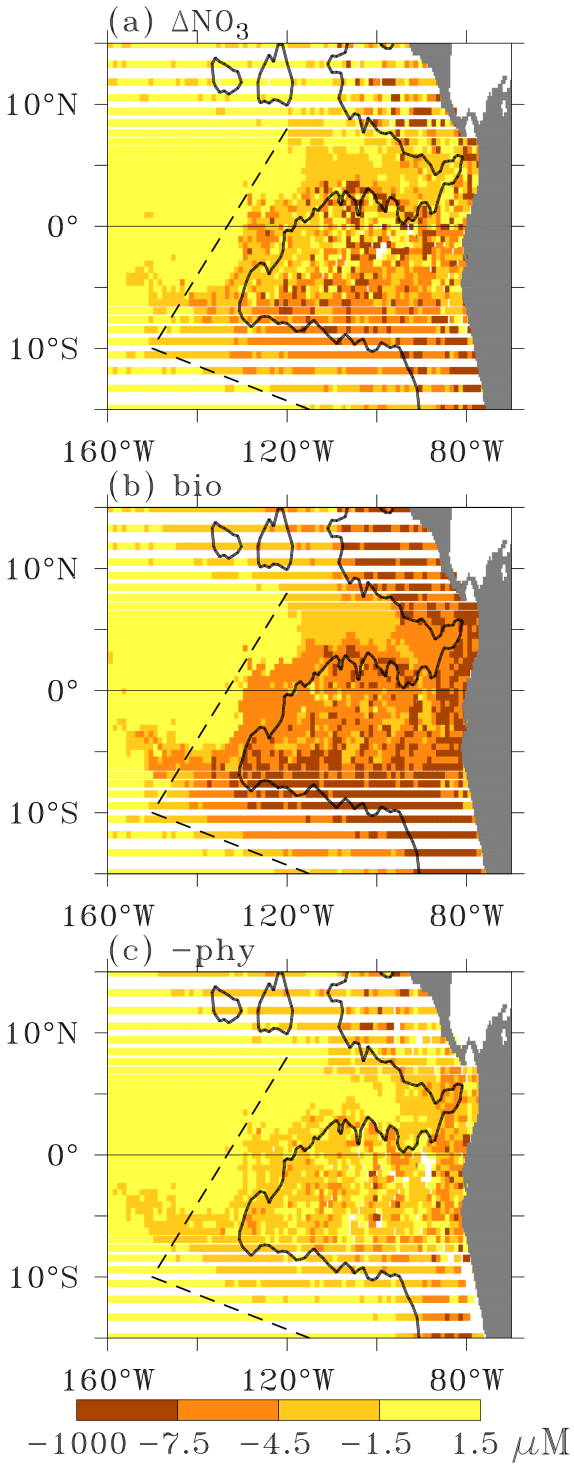

Fig. 7a-c Maps of the (**a**) NO_3 consumption and impacts of the (**b**) biological and (**c**) physical effects (μM; color key) between May and December 1997. The 1 μM surface nitrate isoline (*thick line*) is superimposed. The *dashed line* is the leading edge of eastward spreading 'pre El Niño' oligotrophic waters.

water mass		NO_3	T	latitude	longitude
warm pool	WPW	< 1	≥ 29		≤ 120°W
north-west subtropical	NWSW	< 1	< 29	≥ 0	≤ 180
north-east subtropical	NESW	< 1	< 29	≥ 0	> 180
south subtropical	SSW	< 1	< 29	< 0	
equatorial upwelling	UPW	[1, 12]		[12°S, 10N°]	
coastal upwelling	CW	[1, 12]		> 10°N	> 180
		[1, 12]		< 12°S	> 180
subsurface	SUBS	none of the above with NO3 ≥ 1			

Table 1 Criteria used to define water masses in May 1997: 4 classes of oligotrophic water with NO_3 < 1 μM and 3 classes of nitrate-rich waters.